Monte Carlo simulation of neutral transport in the non–axisymmetric region of the GAMMA 10 anchor–cell

Y. N A K A S H I M A, Y. H I G A S H I Z O N O, M. S H O J I,[1]
S. K O B A Y A S H I,[2] Y. K U B O T A, M. Y O S H I K A W A,
T. K O B A Y A S H I, M. K. I S L A M and T. C H O

Plasma Research Center, University of Tsukuba, Ibaraki 305-8577, Japan
[1]National Institute for Fusion Science, 322-6 Oroshi-cho, Toki, Gifu 509-5292, Japan
[2]Institute of Advanced Energy, Kyoto University, Gokasho, Uji 611-0011, Japan

Abstract. A three-dimensional neutral transport model using the DEGAS version 63 Monte Carlo code is described in order to understand the behavior of neutrals in the non-axisymmetric anchor region of the GAMMA 10 tandem mirror. A precise mesh structure with three-dimensional geometry was built up and the simulation was carried out under a plausible assumption of the particle source on the basis of experimental data. In standard ion-cyclotron-range-of-frequency heated plasmas, detailed measurements of H_α line emission were performed using a 5-ch H_α detector array in the outer-transition region of the east anchor cell and the experimental results were compared with the simulation. The spatial profile of H_α emission predicted from the simulation agreed well with the experimental result and the distinctive behavior of neutrals in this region was clarified.

1. Introduction

Modeling of neutral particle transport is an important issue to investigate hydrogen recycling and transport phenomena in not only the plasma edge regions but also the core plasma of magnetically confined plasmas. Neutral particles in periphery plasmas play a crucial role on plasma transport and recycling phenomena in high-temperature plasmas. In the GAMMA 10 tandem mirror, the neutral transport code DEGAS [1] has been applied and the simulation studies have been performed for investigating the neutral particle behavior in tandem mirror plasmas [2, 3]. Recently a fully three-dimensional neutral transport analysis has been successfully achieved using the DEGAS version 63 code and the complicated behavior of neutrals in the non-axisymmetric region of GAMMA 10 is being revealed [4]. In this paper, details of the neutral transport modeling in the outer-transition region of GAMMA 10 are presented and the comparison between the experiment and the simulation is discussed from the viewpoint of the particle source and the geometry of the plasma in this region.

2. Modeling of the GAMMA 10 anchor cell

GAMMA 10 is an axisymmetric minimum-B anchored tandem mirror with thermal barrier. The device consists of an axisymmetric central-mirror cell, anchor cells
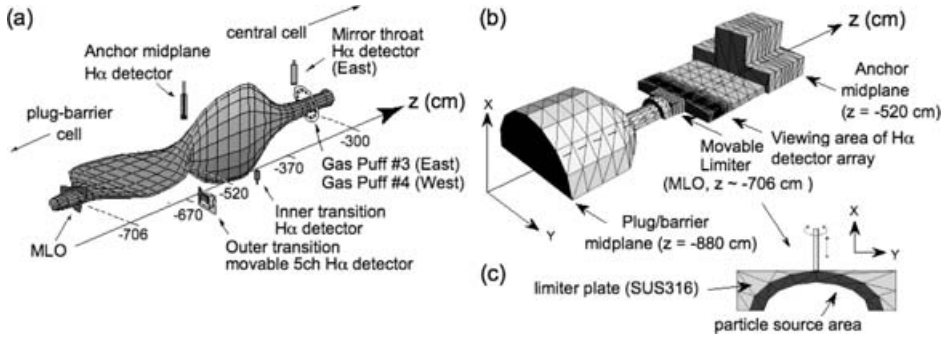
Figure 1. Schematic view of the anchor cell and the mesh structure for the simulation: (a) plasma surface mesh and location of detectors; (b) mesh model of the vacuum chamber wall and the location of a movable limiter (MLO) at the outer-transition region ($z = -706$ cm); (c) schematic of the MLO mesh model.

with minimum-B configuration using baseball coils, and plug/barrier cells with axisymmetric mirrors. In typical ICRF-heated plasmas of GAMMA 10, the plasma parameters are as follows: $n_e \sim 2 \times 10^{12}$ cm^{-3}, $T_i \sim 5$ keV and $T_e \sim 60$ eV.

Figure 1 shows the schematic view of the east anchor cell and the mesh model in the outer-transition region newly constructed for this simulation. The anchor cells are located at both ends of the central cell and each cell is composed of a minimum-B region with a baseball coil and two transition regions which connect the magnetic field line smoothly between the minimum-B region and the neighboring regions. In the figure, the origin of the z-axis is assigned at the central-cell midplane and the direction of the axis is defined towards the west. In the transition region, as shown in Fig. 1(a), the cross section of the plasma is elliptically elongated, which presents a complicated non-axisymmetric structure as well as the vacuum chamber wall.

In this model an up–down symmetry is introduced and the simulation space is divided into 53 segments in the axial direction from the east anchor midplane ($z = -520$ cm) to the east plug/barrier midplane ($z = -880$ cm). In radial and azimuthal directions the simulation space is divided into 11 and 8 segments, respectively. A precise mesh structure is defined in the region -680 cm $\leqslant z \leqslant -660$ cm in order to compare the simulation results with the experimental results measured with the H_α detector array in this location.

A movable limiter of the outer-transition region (MLO) is installed near the connection point between the plug/barrier cell and the anchor cell ($z = -706$ cm), as shown in Fig. 1(b). MLO is inserted into the plasma center at $r_{cc} \sim 11$ cm with an angle of 49° to the z-axis, where r_{cc} represents the reduced radius to the central-cell midplane. The flowing out plasma from the central region intersects MLO in the periphery region ($r_{cc} \geqslant 11$ cm) and is neutralized there. In this simulation, MLO is modeled as the 'second wall' defined independently of the vacuum chamber wall, which has been successfully achieved by modifying the original code [5]. A particle source is given on MLO and is restricted in the area from $r_{cc} = -11$ to -16 cm (shaded area in Fig. 1(c)).

3. Simulation results and discussion

Figure 2 shows the simulation result of neutral density profiles in the east outer-transition region. The hydrogen molecular density becomes high in the vicinity of
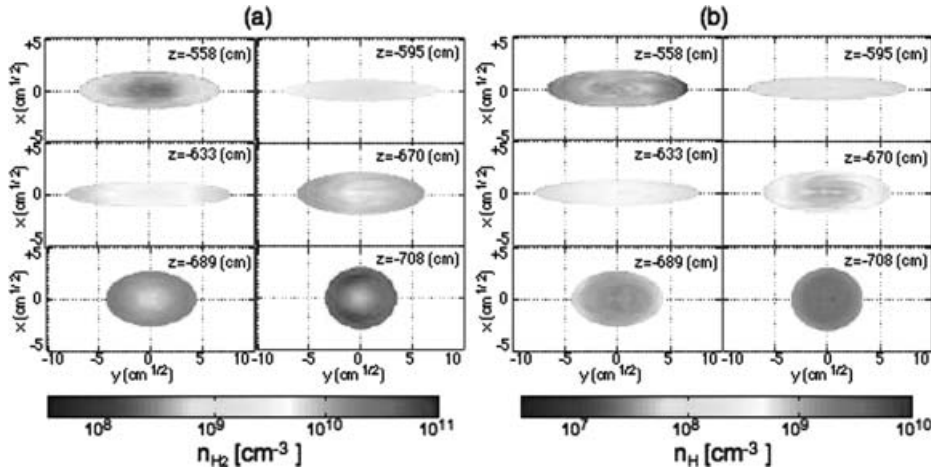
Figure 2. Neutral density profiles determined from the three-dimensional neutral transport simulation using DEGAS: (a) molecular hydrogen density; (b) atomic hydrogen density.

MLO ($z = -708$ cm) and gradually decreases with the distance towards the anchor midplane. The on-axis density reduces by more than one order of magnitude at the entrance of the minimum-B region ($z = -558$ cm) nearly 140 cm away from MLO. The molecular density also decreases from the plasma edge to the core region. Note that this tendency remains unchanged near the region where the plasma cross section becomes flat ($z \sim -595$ cm) even though the length of the plasma diameter (~ 5 cm) is shorter than the mean free path length of neutrals (>10 cm). The hydrogen atom density shown in Fig. 2(b) represents similar behavior to that of molecules along the axial direction. In the radial distribution, in contrast, the density increases towards the plasma center. This behavior can be explained by the fact that the production rate of atomic hydrogen becomes large in the plasma core region, since the electron density has a peak on the axis and the molecules penetrate deeply into the plasma due to the low electron density.

Based on the above simulation results, the spatial profiles of the average neutral density $\langle N_0 \rangle$, the averaged emissivity $\langle \epsilon_{H_\alpha} \rangle$ and the intensity I_{H_α} of H_α line emission are evaluated. In this calculation, each value is determined according to the following formulas:

$$\langle \epsilon_{H_\alpha} \rangle = \sum_x \sum_y \epsilon_{H_\alpha} \cdot v_{\text{mesh}} \bigg/ \sum_x \sum_y v_{\text{mesh}}, \quad I_{H_\alpha} = \sum_y \epsilon_{H_\alpha} \cdot \Delta y,$$

$$\langle N_0 \rangle = \sum_x \sum_y \epsilon_{H_\alpha} \cdot v_{\text{mesh}} \bigg/ \sum_x \sum_y n_e \cdot v_{\text{mesh}},$$

where v_{mesh} is the plasma volume of each mesh in the simulation space and Δy is the unit length in the observation line of sight.

Figure 3 shows the comparison with the experimental results. The vertical (x-direction) profile of the H_α line intensity measured at $z = -670$ cm (triangles in Fig. 3(a)) corresponds well with the simulation in the core region. In the edge region, however, a clear discrepancy is observed. This difference is thought to be caused by uncertainty in the edge plasma parameters and by the effect of the scrape-off-layer plasma ($r_{cc} > 20$ cm) which is not taken into account in the simulation.
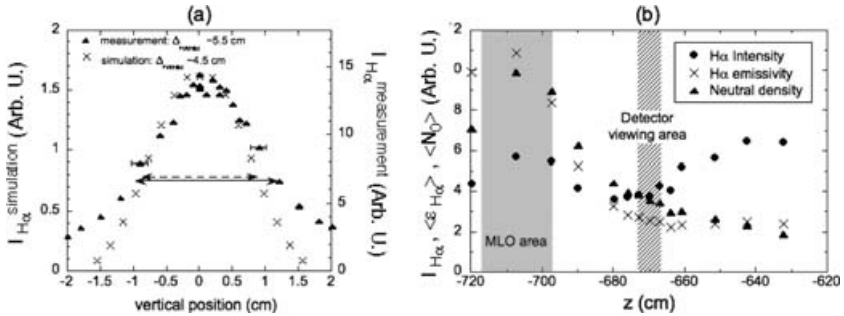
Figure 3. (a) Vertical profile of the H_α line intensity; (b) axial profile of H_α intensity, emissivity and neutral density obtained from the simulation.

Figure 3(b) shows the simulation results of axial profiles of $\langle N_0 \rangle$, $\langle \epsilon_{H_\alpha} \rangle$ and I_{H_α}. As shown in the figure, the neutral density reaches a maximum at the MLO position and promptly decreases towards the anchor midplane. The emissivity of the H_α line also decreases similarly. These results indicate the influence of the particle source due to hydrogen recycling on MLO. On the other hand, the extent of the decrease in the H_α line intensity is small compared with those of the neutral density and emissivity. The intensity becomes minimum in the vicinity of the viewing area of the detector and increases again in the direction of the anchor midplane. This behavior can be interpreted in such a way that the increasing diameter of the plasma cross section along the line of sight of the detector compensates for the decrease of the emissivity with the distance to MLO, since the length of the line of sight at the inner side of the viewing area ($z = 660$ cm) becomes five times as long as that at the MLO area ($z = 710$ cm). This result also agrees well with the experimental results [6].

4. Summary

Neutral particle transport modeling was successfully performed over the region from the minimum-B anchor cell to the axisymmetric plug/barrier cell of the GAMMA 10 tandem mirror for the first time, using the DEGAS Monte Carlo code. Based on the simulation results, H_α emissivity and its intensity near the observation area were evaluated and the simulation results matched the experimental results very well. From the above results, it is clarified that the three-dimensional Monte Carlo simulation of neutral particle transport provided interesting phenomena on neutral density profiles in the non-axisymmetric anchor minimum-B region of GAMMA 10. This analysis method also gives us important information for the three-dimensional plasma modeling of other plasma devices in the near future.

References

[1] Heifetz, D. et al. 1982 *J. Comput. Phys.* **46**, 309.
[2] Nakashima, Y. et al. 1992 *J. Nucl. Mater.* 196–198, 493.
[3] Nakashima, Y. et al. 1997 *J. Nucl. Mater.* 241–243, 1011.
[4] Nakashima, Y. et al. 2004 *J. Plasma Fusion. Res. SERIES* **6**, 546.
[5] Nakashima, Y. et al. 2005 *J. Nucl. Mater.* 337–339, 466.
[6] Higashizono, Y. et al. 2005 *Trans. Fusion Sci. Technol.* **47**, 297.